ELSEVIER

Journal of Structural Geology 30 (2008) 478–490

JOURNAL OF STRUCTURAL GEOLOGY

www.elsevier.com/locate/jsg

Escape of fluid-driven fractures from frictional bedding interfaces: A numerical study

Xi Zhang [a,*], Robert G. Jeffrey [a], Marc Thiercelin [b]

[a] CSIRO Petroleum Resources, Bayview Avenue, Clayton, VIC 3168, Australia
[b] Schlumberger RTC-Unconventional Gas, 14131 Midway Road, Suite 700, Addison, TX-75001, USA

Received 13 June 2007; received in revised form 30 October 2007; accepted 5 December 2007
Available online 14 December 2007

Abstract

Fluid-driven or hydraulic fractures, either natural or man-made, which are propagating vertically in horizontally layered rocks, may interact with and deflect into bedding interfaces that they intersect. Pre-existing secondary flaws located along the frictional bedding contact defined as the bedding plane, can serve as nucleation sites for new fractures that are extended first by interface slip and then by fluid. If the flaw propagates, a stepped fracture forms. In this paper, a two-dimensional numerical fracture model is used to analyse the coupled rock deformation and fluid flow in such fractures. Numerical results show that fracture escape from the interface is likely under the conditions of fracture growth from stiff to soft rocks, small layer-to-layer far-field stress contrasts, and moderately low fluid viscosity, and small parent fracture lengths and offset distances. The change of the fracture propagation direction at the bedding plane gives rise to a variety of fracture and fluid flow patterns. Fracture permeability and internal pressure vary with time and location. Vertical fracture growth can impede fluid flow along the offset by inducing additional compressive stress on it. If the offset channel is of relatively large permeability, most fluid will be directed into the new fracture to facilitate fracture escape. Alternatively, the interaction and geometry of the fracture branches can lead to low opening compliance on the offset and localised pinching of the fracture surfaces, which restrict fluid flow.
© 2007 Elsevier Ltd. All rights reserved.

Keywords: Fluid-driven joint; Hydraulic fracture; Bedding interface; Secondary flaw; Numerical modelling

1. Introduction

Examples of fluid-driven fractures range from man-made hydraulic fractures used to stimulate oil and gas wells to natural hydraulic fractures such as volcanic dykes and some joints. When such opening-mode fluid-driven fractures propagate in layered rock, they will inevitably encounter and intersect some weak layer interfaces. In this paper these weak bedding interfaces, also referred to as frictional bedding planes, are considered to be highly idealized mechanical surfaces and we neglect much of the diversity and complexity of bedding contacts as they occur in nature. The frictional interface, which may have initial fluid conductivity, can transmit compressive normal stress, but not tensile stress.

Fracture crosscutting and offsetting in the presence of bedding interfaces have been documented both for natural hydraulic fractures (Pollard, 1973; Pollard and Aydin, 1988; Helgeson and Aydin, 1991; Lacazette and Engelder, 1992; Gross, 1993; Renshaw and Pollard, 1995; Cooke and Underwood, 2001) and for man-made hydraulic fractures (Teufel and Clark, 1984; Warpinski and Teufel, 1987; Van As and Jeffrey, 2000). Particularly, the motivation for this study stems from a lack of understanding of the process for hydraulic fractures to cross-interfaces in layered rocks. Containment of commercial hydraulic fractures within a layer is often a desired outcome of oil and gas stimulation treatments, as well as for CO_2 sequestration operations (Teufel and Clark, 1984). Alternatively, some designs assume that the hydraulic fracture can penetrate frictional interfaces, such as the case in the preconditioning of rock masses for

* Corresponding author. CSIRO Petroleum Resources, Private Bag 10, Bayview Avenue, Melbourne, Clayton, VIC 3168, Australia. Tel.: +61 3 95458388; fax: +61 3 95458380.
E-mail address: xi.zhang@csiro.au (X. Zhang).

0191-8141/$ - see front matter © 2007 Elsevier Ltd. All rights reserved.
doi:10.1016/j.jsg.2007.12.001

mining by caving methods, which requires the hydraulic fracture to penetrate natural fractures and bedding interfaces (Van As and Jeffrey, 2000). The ability to predict fracture growth in a naturally fractured or layered rock is of significant scientific and industrial interests.

Fracture interaction with and re-initiation from a frictional interface has received considerable attention. Weertman (1980) and Keer and Chen (1981) analysed the effect of interface slip on aperture distribution along a uniformly pressurised fracture. In these studies, large slip along the interface acts to blunt the fracture tip, although the distribution of shear stresses was assumed *ad hoc*. Gudmundsson and Brenner (2001) considered the mechanisms of hydraulic fracture arrest at closed interfaces in layered host rocks, with various distributions of fluid pressure, including an unpressurised fluid lag zone behind the tip. Finite element analyses of the stress fields for a strongly bonded interlayer were carried out by Helgeson and Aydin (1991) and Fischer et al. (1995). The interlayer plays a fundamental role in limiting vertical fracture growth and physical continuity of fracture and joint traces. However, the weak bedding contacts are also important to fracture termination and step-over as discussed by Cooke and Underwood (2001). Cooke and Underwood (2001), in particular, have considered the cases where the weak interface can slide when its frictional strength is exceeded by shear stress. They found that localised opening, rather than sliding on the interface near the intersection point, is responsible for fracture termination and offsetting, which they call step-over. Following Helgeson and Aydin (1991), the offset that we use to describe the sidestep trace geometry of the composite fractures is not associated with any process or generating mechanism. Later, we show that slip and opening can occur simultaneously along the step-over or the offset. Zhang et al. (2007) have numerically dealt with the fracturing process involving coupled rock deformation and fluid flow along a frictional interface. Their numerical results showed that fracture aperture and frictional sliding vary with time, material parameters and *in situ* stresses. At early stages of fracture growth along the interface, evolving fracture and fluid flow patterns lead to portions of the fracture with reduced opening that act to impede fluid flow. This directly results in lower fracture permeability, higher fluid pressure and an associated increased probability for fracture arrest or direct crossing of the interface.

The hydraulic fracture or joint growth along the interface can eventually be directed into secondary flaws which may serve as a site for fracture re-initiation and allow the hydraulic fracture to escape the interface. Complicated vertical fracture patterns are presented by Underwood et al. (2003) in their fracture maps of outcrops in Silurian dolomite, north Wisconsin. The joints exhibited statistical distances of offsets, strongly suggesting fracture nucleation from the pre-existing flaws. Additionally, in the layered siltstones and shale of the Appalachian Plateau, central New York, joint nucleation locations are always at pre-existing flaws such as fossil inclusions, pyrite concretions, voids, cusps and burrows along bedding interfaces (Bahat and Engelder, 1984; McConaughy and Engelder, 2001). With fracture re-initiation from a randomly located flaw, favourable local stress conditions allow the new fracture to grow further (Pollard and Aydin, 1988), and potentially to form an offset fracture path which is left behind as the fracture escapes the bedding interface. Interface sliding transferred from the vertical fracture opening can cause a small flaw to grow into the intact upper rock for a short distance without the aid of pressurised fluid. However, higher *in situ* layer-parallel compression in the upper rock may prevent new fracture growth until fluid entering the new fracture provides sufficient driving force. In general, the escape of a fluid-driven fracture from a bedding interface depends on a number of factors such as interface orientation with respect to the remote stress field, far-field stress levels, fracture sizes, fracture toughness contrasts, interface frictional coefficients and rock and fluid properties.

This paper examines numerically the escape of a fluid-driven fracture from a frictional bedding interface via mechanisms associated with growth of a pre-existing flaw, which is assumed to exist at a random location along the bedding interface. The frictional behaviour of the bedding interface is assumed to obey the Coulomb frictional law with zero cohesion. Furthermore, the parent hydraulic fracture is assumed to be perpendicular to the horizontal frictional interface and the principal far-field stresses are chosen so that the fracture initially grows vertically. The hydraulic fracture propagation is driven by an incompressible, Newtonian fluid supplied at a constant injection rate, while the rock layers are elastic and impermeable. The injection rate and viscosity used are such that viscous dissipation is important for all cases presented. A boundary element model is used to explicitly treat the coupling mechanisms of fracture propagation and fluid flow.

The remainder of this paper is organised as follows: in Section 2 the problem is formulated and the geometric settings, loading and boundary conditions are given, as well as the governing equations. Section 3 contains a validation of the proposed numerical method especially for fracture kinking out of the interface. Numerical simulations of fracture escaping scenarios in homogeneous and heterogeneous rock layers are presented in Section 4 considering flaw location, fracture length, *in situ* stress, and rock and fluid properties. Section 5 concludes the paper with a discussion of fluid-driven fracture escaping mechanics and processes.

2. Problem formulation

Consider, as shown in Fig. 1(a), an initially vertical fluid-driven fracture that has intersected and is propagating along an interface between two linear-elastic half-planes. The problem is treated as two-dimensional based on the plane-strain assumption that implies the fracture is infinitely long in the z-direction. A Cartesian coordinate system is used with the y-axis lying along the bedding interface that is closed initially. The origin of the coordinate system shown in Fig. 1(b) is at the point where the parent fracture eventually intersects the interface. The fluid injection point is at a distance L from the intersecting point. The hydraulic fracture is allowed to propagate only towards the bedding interface, while growth in the

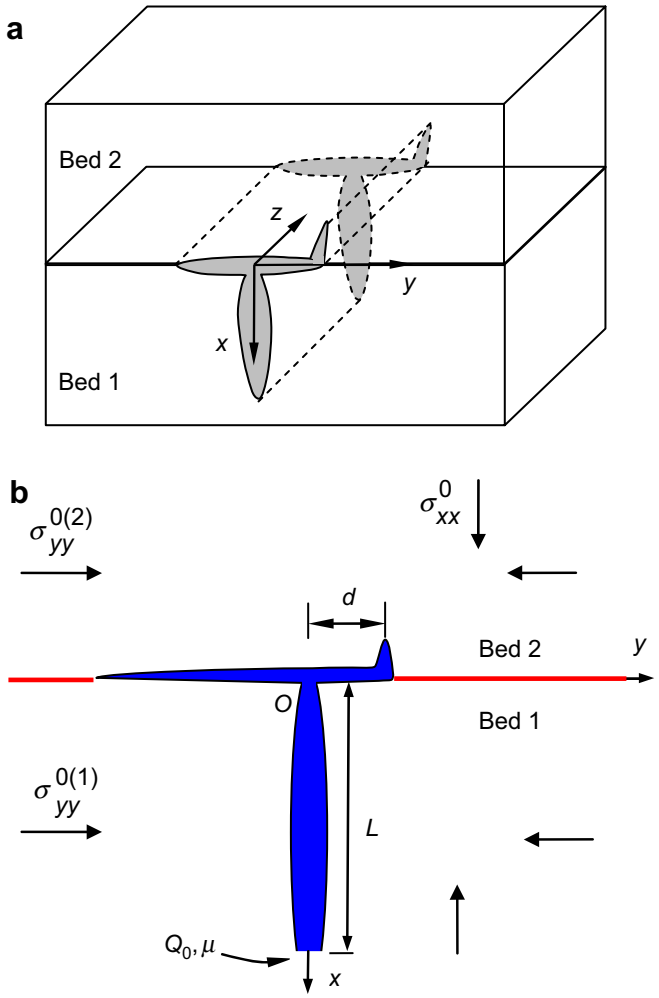

Fig. 1. Schematic of geometry used to examine escape of a fluid-driven fracture from a frictional interface with defined coordinate system and controlling parameters. (a) Three-dimensional and (b) plane-strain.

direction away from the interface is arbitrarily prevented. The frictional interface is discretised using fracture elements with assigned frictional properties and zero fracture toughness. As the size of this discretised interface is much larger than other length scales of the configuration shown in Fig. 1(b), the problem as defined is equivalent to the fracture interacting with an infinitely long interface. In addition, a pre-existing vertical secondary flaw of a small length exists at a distance d from the intersecting point. The vertical far-field stress is σ_{xx}^0 and the horizontal far-field stresses in the lower and upper half-planes are $\sigma_{yy}^{0(1)}$ and $\sigma_{yy}^{0(2)}$, respectively. $\sigma_{yy}^{0(1)}$ and $\sigma_{yy}^{0(2)}$ are both smaller than σ_{xx}^0 so that the natural hydraulic fracture will prefer to propagate vertically. The Young's moduli, Poisson's ratios and fracture toughness for each layer are, respectively, E_i, ν_i and K_i^C, where subscript i denotes the layer $i = 1, 2$.

Elasticity provides a relationship between the normal, w, and shear, v, displacement discontinuities (DDs) of the fracture walls and the fluid pressure p_f or other tractions acting on the fracture surface. Fluid pressure and far-field stresses are taken as positive if in compression. The elasticity equation is established using a superposition technique of singular dislocation dipole solutions. Summing up the contribution of all fracture branches to the stress level at a specific location of each fracture, the elasticity equation of equilibrium in the framework of a Cartesian coordinate system is

$$\begin{aligned}\sigma_n(\boldsymbol{x},t)-\sigma_1(\boldsymbol{x}) &= \sum_{r=1}^{N}\int_0^{\ell_r}[G_{11}(\boldsymbol{x},s,\alpha,\beta)w(s)\\ &\quad + G_{12}(\boldsymbol{x},s,\alpha,\beta)v(s)]\mathrm{d}s\\ \tau_s(\boldsymbol{x},t)-\tau_1(\boldsymbol{x}) &= \sum_{r=1}^{N}\int_0^{\ell_r}[G_{21}(\boldsymbol{x},s,\alpha,\beta)w(s)\\ &\quad + G_{22}(\boldsymbol{x},s,\alpha,\beta)v(s)]\mathrm{d}s\end{aligned} \tag{1}$$

where $\boldsymbol{x} = (x, y)$ and t is time; $\mathrm{d}s$ is the infinitesimal arc length along the fracture; ℓ_r is the fracture length with a subscript index r identifying the fracture branch; σ_n is the normal stress and, within the fluid-filled parts, it is equal to p_f; τ_s is the shear stress associated with the frictional sliding along the interface; σ_1 and τ_1 are the normal and shear stresses along the fracture plane at $\boldsymbol{x}$ generated by the far-field stresses; and G_{11}, G_{12}, G_{21}, G_{22} are hypersingular Green's functions as given by Zhang and Jeffrey (2006). These Green's functions are dependent on the Dundurs' parameters, which are defined by

$$\alpha = \frac{\mu_2(\kappa_1+1)-\mu_1(\kappa_2+1)}{\mu_2(\kappa_1+1)+\mu_1(\kappa_2+1)};\quad \beta = \frac{\mu_2(\kappa_1-1)-\mu_1(\kappa_2-1)}{\mu_2(\kappa_1+1)+\mu_1(\kappa_2+1)} \tag{2}$$

where $\kappa_i = 3 - 4\nu_i$ and ν_i $(i = 1, 2)$ are Poisson's ratios for the upper and lower layers.

In order to maintain continuity of layer-parallel normal strains across the interface, the stresses $\sigma_{yy}^{0(1)}$ and $\sigma_{yy}^{0(2)}$ are related by (Rice and Sih, 1965)

$$\frac{\sigma_{yy}^{0(2)}}{\sigma_{yy}^{0(1)}} = \Gamma + \left(\frac{\nu_2}{1-\nu_2} - \Gamma\frac{\nu_1}{1-\nu_1}\right)\frac{\sigma_{xx}^0}{\sigma_{yy}^{0(1)}} \tag{3}$$

where $\Gamma = E_2(1-\nu_1^2)/E_1(1-\nu_2^2)$. The stress ratio $\sigma_{yy}^{0(2)}/\sigma_{yy}^{0(1)}$ is referred to as the stress contrast across the interface.

The fluid flow in the fracture is governed by the lubrication equation (Batchelor, 1967):

$$\frac{\partial w}{\partial t} = \frac{\partial}{\partial s}\left(\frac{w^3}{\mu'}\frac{\partial p_f}{\partial s}\right) \tag{4}$$

where $\mu' = 12\mu$ and μ is the fluid viscosity. There is no fluid loss into the rock during the fracturing process since the rock is assumed impermeable. The global mass balance for injected fluid then leads to

$$\sum\int_0^{\ell_f} w\,\mathrm{d}s = Q_0 t \tag{5}$$

where ℓ_f is the fluid penetrated length of each fracture and Q_0 is the fluid injection rate. The formulation also accounts for

a fluid lag, which is the distance between the fluid front and the fracture tip for each fracture branch. The fluid front velocity can be found in terms of the flux $q(\ell_f)$ and the opening $w(\ell_f)$ at each fluid front in the form of

$$\dot{\ell}_f = \frac{q(\ell_f)}{w(\ell_f)} \tag{6}$$

where the flux is $q = (w^3/\mu')(\partial p_f/\partial s)$, based on Poiseuille's law.

The sum of fluid fluxes for all fractures connecting to the injection point is equal to the injection rate, that is,

$$\sum q(0) = Q_0 \tag{7}$$

At each fracture tip, the opening and shearing DDs vanish, that is,

$$w(\ell) = v(\ell) = 0 \tag{8}$$

However, when the open hydraulic fracture tip is on the frictional interface, a non-zero shear DD may exist.

The magnitudes of the Mode I and II stress intensity factors are determined by the displacement correlation method. In order to determine the fracture trajectory, the commonly-used failure criterion (Erdogan and Sih, 1963) is adopted, in which the fracture propagates along the direction of maximum tensile hoop stress. Specifically, if both Mode I and II stress intensity factors are known, the fracture propagation direction is determined by solving the following equation:

$$K_I \sin\Theta + K_{II}(3\cos\Theta - 1) = 0 \tag{9}$$

and the condition for fracture growth is given as

$$\cos\frac{\Theta}{2}\left(K_I \cos^2\frac{\Theta}{2} - \frac{3}{2}K_{II}\sin\Theta\right) = K^C \tag{10}$$

where Θ is the deflection angle from the current fracture propagation direction, K_I and K_{II} are the Mode I and II stress intensity factors, respectively, and K^C is the rock toughness of the layer in which the fracture tip is located.

The numerical scheme for fracture coalescence with the interface has been described by Zhang et al. (2007). The frictional behaviour of interfaces obeys Coulomb's law without cohesion (Jaeger and Cook, 1979). The numerical method for treating frictional contacts has also been given by Zhang et al. (2007). In addition, the numerical method enforces continuity of fluid pressure and conservation of flux at the parent fracture–interface and flaw–interface intersections as discussed by Zhang et al. (2007). Although bedding interfaces are idealized as smooth and continuous, they are allowed to posses an initial permeability embodied in an initial aperture, w_o^h. This aperture is not a mechanical opening that induces stress changes, but is only used in the fluid flow calculations. The resulting conductivity can help a fluid-driven joint to initially enter a closed interface since the fluid can more easily enter interfaces that possess an initial conductivity. In addition, transient flow along such interfaces with the initial conductivity is not yet considered in the model, and fluid flow is based on the assumption of steady state flow. The fluid front is therefore not allowed to extend beyond the edge of the mechanically open region on the interface. Also, the interface conductivity associated with w_o^h is preserved if the interface is closed again because of stress changes arising during fracture crossing.

3. Numerical model

Our numerical modelling uses a two-dimensional boundary element program named MineHF2D, which can deal with fluid flow and elastic rock deformation for hydraulic fracture propagation in the presence of interfaces that may undergo frictional slip. The details of the numerical algorithm are given in our previous papers (Zhang et al., 2005, 2007). The interface and the fracture are discretised into straight elements of equal length, each of which can support constant normal and shear DDs. By using a sufficient number of small elements, the variations of fracture wall displacements can be obtained within any desired accuracy. MineHF2D has previously been used to model the main features associated with interactions between fluid-driven fractures and interfaces without considering the development of new fractures from the flaws (Zhang et al., 2007). These results have been compared with published existing results and were proven to be accurate.

For modelling the escape of a fracture from an interface, the fracture kinking process must be modelled accurately. As an example test of the numerical model, let us consider a kinked fracture growing at various kink angles from a semi-infinite interfacial fracture as studied by He et al. (1991). In this case, the length of the kink fracture is extremely small compared with the interfacial fracture. The extremely small length ratio of the elements for the kinking segment and the interface can cause numerical instability. The element sizes for both kinked and interfacial portions were then chosen by restricting the ratio of their element sizes to be larger than 0.05, in order to obtain the accurate numerical results as presented in Fig. 2. Our numerical results of the stress intensity factors fall well within the envelopes generated by He et al. (1991) who used a Chebyshev-polynomial based numerical method to solve the integral equation associated with equilibrium of the kinked fracture.

4. Modelling results

A composite joint or fracture can be split into multiple fracture segments. In this paper, the parent fracture refers to the segment covering the distance from the injection point to the intersection point, while the new (daughter) fracture refers to the fracture portion in the upper layer starting from the secondary flaw. The fluid-filled interface portion can be divided into two parts. One portion is the offset that connects the parent and the new fracture, and the other is the fluid-loss branch on either or both sides of the offset where any stored fluid volume reduces the fluid flux into the daughter fracture.

Considering local opening changes at the fracture junctions, there are four possibilities that result in either limiting or aiding fluid flow into the new fracture. If the fracture aperture

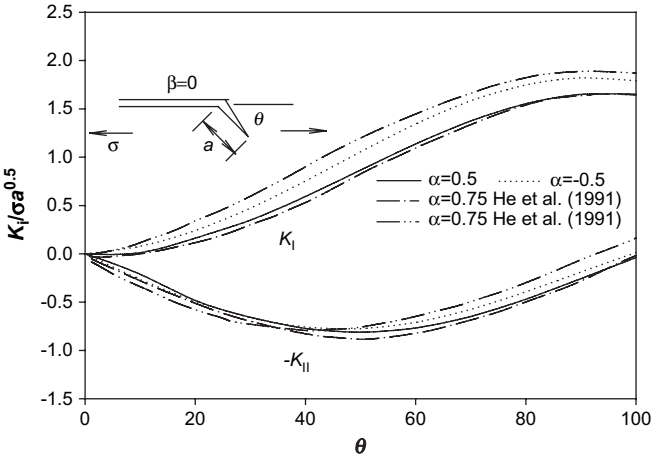

Fig. 2. Angular dependence of Mode I and II normalised stress intensity factors for a kink fracture out of a semi-infinite interfacial fracture under the far-field stress σ parallel to the interface. The curves for Dundurs' parameter $\alpha = -0.75, 0.75$ are extracted from He et al. (1991) to show the bounds of the numerical results.

along the pathway leading to the new fracture is narrowed in time, the fracture escape from interface will be retarded or prevented. The situation in Fig. 3(a) has been considered by Zhang et al. (2007), where the fracture aperture reduction is developed near the intersection site because of relatively high confinement across the interface. Depending on the frictional strength of the interface, the parent fracture is either blunted and stops at the interface or, alternatively, penetrates straight through a frictionally strong interface.

Here, we consider cases where the offset is opened by the hydraulic fracture as illustrated in Fig. 3(b–d). After the new fracture grows, either induced by interface sliding or driven by fluid, the symmetry of the fracture geometry is lost. This can give rise to stress perturbation and shearing deformation along the parent fracture. In Fig. 3(b), the shearing along the parent fracture surface and interaction stress changes result in sealing of the fluid-loss branch. The total flow out from the parent fracture will be directed into the offset and then into the new fracture. Another possibility is that a pinching point develops on the offset that limits fluid flow into the new fracture. For instance, a pinch point can develop as shown in Fig. 3(c), resulting from the mechanical interaction between the interface fracture and a relatively long and wide new fracture. Such an impediment to fluid flow can cause fluid flow diversion into the fluid-loss branch until the pinch point shown in Fig. 3(b) is relaxed or opened by pressure. This pinch on the offset can be opened by the continued growth of the fluid-loss branch, which promotes increased opening on the interface. Alternatively, the fluid-driven fracture may permanently be trapped on the interface, as shown in Fig. 3(d). Continuous fracture growth from the flaw might well not occur in this case because fracture growth along the interface can occur more easily. In short, the problem being addressed is complicated since the stress and deformation states evolve as a result of the coupling of rock deformation and fluid flow.

Results will be presented for a set of parameter values for typical rocks such as granite and sandstone with elastic properties $E = 20$ GPa, $\nu = 0.15$, $K^C = 1.1\ \mathrm{MPa}\sqrt{m}$ for the sandstone and $E = 40$ GPa, $\nu = 0.15$, $K^C = 1.7\ \mathrm{MPa}\sqrt{m}$ for the granite, if not otherwise specified. The coefficient of interface friction is $\lambda = 0.5$ and the initial interface aperture is $w_o^h = 0.1$ mm. A constant injection rate $Q_0 = 0.006\ \mathrm{m}^2/\mathrm{s}$ is used and the fluid dynamic viscosity is $\mu = 0.1$ Pa s if not specified separately. Firstly, we will investigate development of new fractures for two homogeneous sandstone layers to explore some basic features of fluid-driven fracture propagation across a frictional interface. Next, we present parametric studies of the effect of the offset size, fracture length, *in situ* stresses and fluid viscosity on the formation of composite joints in granite/sandstone layers.

4.1. Fractures in homogeneous sandstone layers

To evaluate the influence of fluid transport on fracture offsetting at the bedding interfaces, we consider fracture

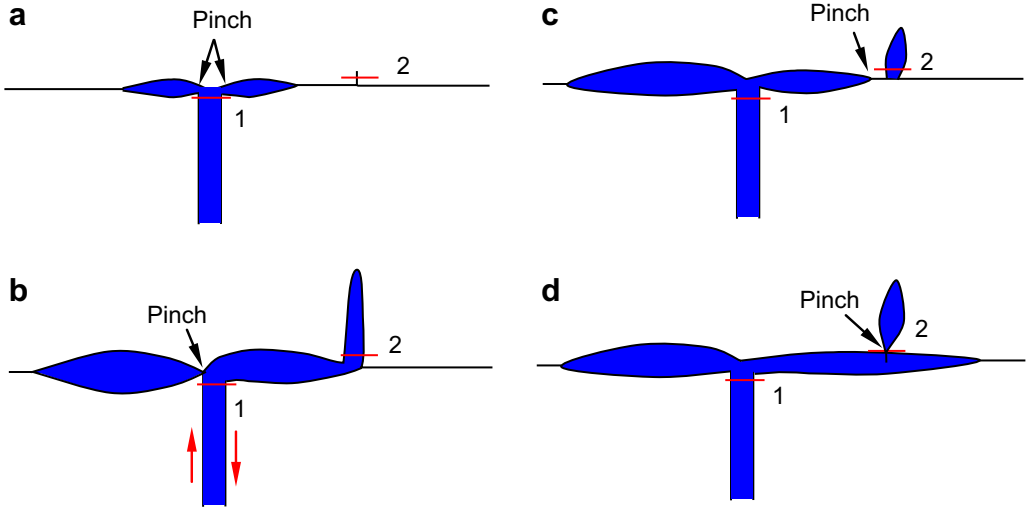

Fig. 3. Four possibilities associated with the formation of pinches along fluid-driven fracture pathways. Points 1 and 2 as indicated represent the ending point of the parent joint and the mouth of the new daughter fracture, respectively.

propagation in layers of homogeneous sandstone, separated by a frictional interface, as shown in Fig. 4. The vertical and horizontal remote field stresses are 12 and 5 MPa, respectively. The time Δt starts when the parent fracture tip reaches the interface. The fracture trajectories at time $\Delta t = 0.6$ s are given for $d = 0.05$, 0.1 and 0.5 m in Fig. 4(a). The flaw most remote to the intersection point produces an inclined new fracture with respect to the interface, while the closer flaws generate new fractures nearly perpendicular to the bedding contact. It is possible that the interface opening left of the daughter fracture is sufficient to induce shearing along the daughter fracture that would change fracture propagation direction. The larger offset distance would produce a larger interface opening portion and a more inclined new fracture. As shown in Fig. 4(a), the nearly vertical new fractures propagate somewhat faster, based on their length, than the inclined fracture.

Importantly, the model calculates the variations of normal stresses with time and location, as shown in Fig. 4(b) in the case of $d = 0.1$ m. The insert is an enlarged plot for the area around the offset. Along the interface, the normal stress plotted above the interface represents the fluid pressure and, below the interface, the contact stress. Along the parent and daughter fractures, only the pressure is plotted. The non-zero pressure along the parent and the daughter fractures indicates the fracture portion occupied by injected fluids. The fracture elements are drawn as small squares and there is no contact stress (only pressure) along the offset. At $\Delta t = 0.6$ s, the fluid pressure is nearly constant in the parent fracture. Close to the new fracture tip, there is a lag zone without fluid, as discussed by Zhang et al. (2005). The fluid pressure distribution in the new fracture exhibits a gradient near the fluid front, typical of hydraulic fractures. In addition, the pressure distribution reflects a strong gradient along the offset portion. The offset is mechanically stiff with respect to generation of fracture aperture from internal pressure. Additional compressive stress is induced on the interface by the parent and daughter fractures. The large pressure loss in the presence of the offset is an important feature associated with hydraulic fracture crossing. In addition, the

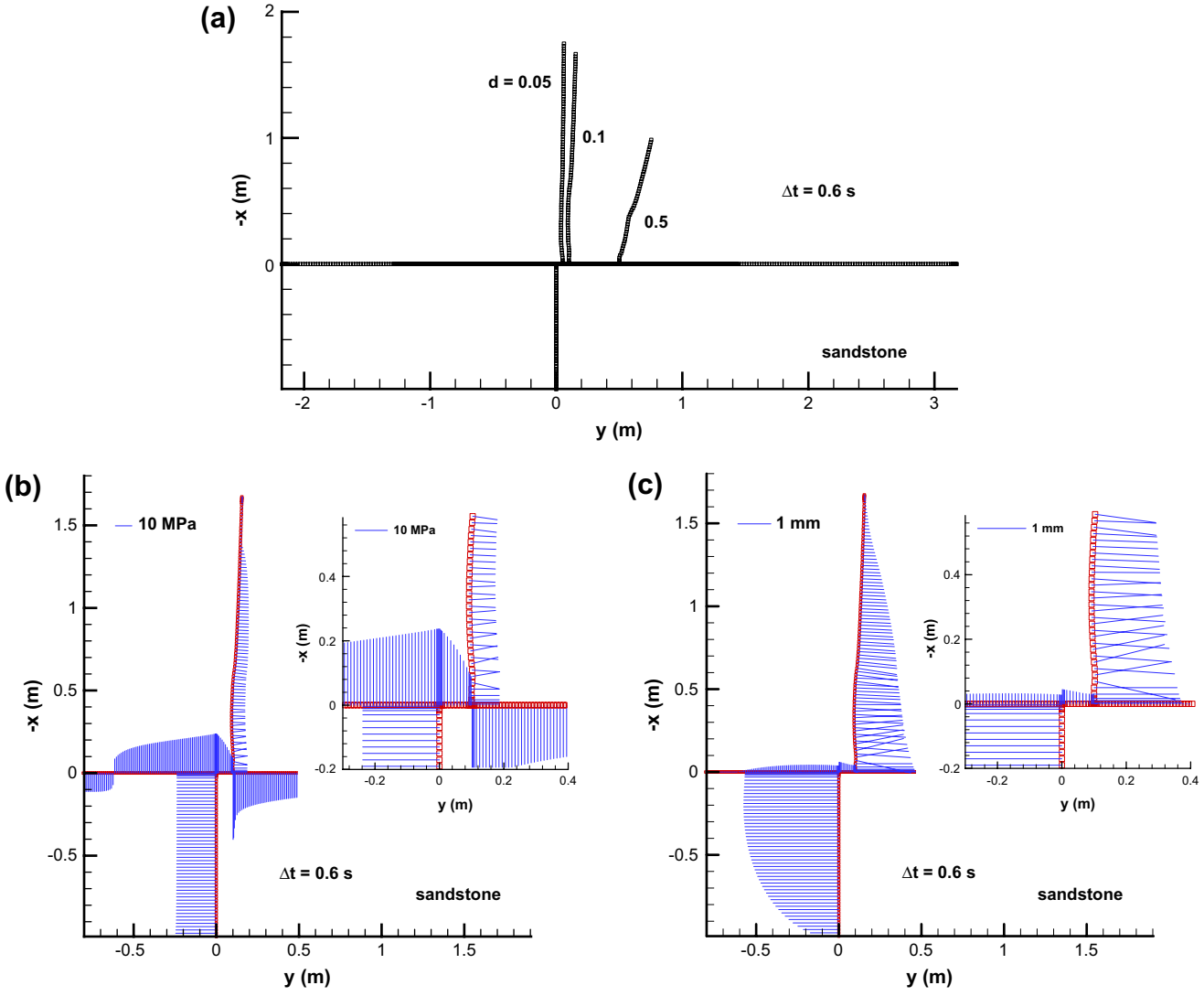

Fig. 4. The effects of fluid flow on fracture propagation behaviours in bedded sandstones. (a) The new fracture pathways for various flaw sites at $\Delta t = 0.6$ s. Distributions of (b) normal stress and (c) fracture aperture along the joints and the interface at $d = 0.1$ m ($\mu = 0.1$ Pa s, $L = 1$ m, $\sigma^0_{xx} = 12$ MPa, $\sigma^{0(1)}_{yy} = \sigma^{0(2)}_{yy} = 5$ MPa).

enhancement of confining stress across the interface is also reflected in an increase of interfacial contact stress to the right of the daughter fracture. If an uncoupled model that does not include viscous dissipation (e.g. uniform pressure) were to be used, the fracture growth and resulting geometry would be expected to be different from that shown in Fig. 4. As the pressure must be higher than the remote vertical stress, unstable growth of the new fracture will be predicted based on a uniform pressure model. Only by allowing the offset portion to close with fluid flow occurring through it by percolation can the daughter fracture propagate in a stable manner. Our model is not currently able to consider such percolation flow.

The profile of fracture aperture is shown in Fig. 4(c). Also, the details near the offset are given in the insert. It is clear that the aperture along the interface is much less than that along the parent and the daughter fractures. The small fracture aperture along the offset is responsible for the large pressure drop. The pressure gradient is increased for a narrow fracture channel that is carrying the relatively large flow rate. Along the interface to the right of the flaw, the fracture aperture is zero. This is consistent with the large clamping stress to the right of the flaw as shown in Fig. 4(b). Along the interface to the left of the parent fracture, there is a significant interface portion ($-0.6\ \text{m} < y < 0$) occupied by fluid. The fluid stored in this section does not contribute to growth of the daughter fracture. The associated reduction of fluid flux into the offset and then into the daughter fracture will lower the pressure and fracture growth rate of the daughter fracture.

Let P_{f1} and P_{f2} denote the normal stresses at two Points 1 and 2 as indicated in Fig. 3, which represent the ending point of the parent fracture and the mouth of the new daughter fracture, respectively. Since relatively constant pressure is achieved in the parent fracture as shown in Fig. 4(b), the value of P_{f1} is approximately taken as the injection pressure or the fracture treatment pressure for man-made hydraulic fractures. In addition, the arrival time of the first fluid pressure at Point 2 is the elapsed time for the fluid front to reach the mouth of the flaw and P_{f2} is proportional to the driving force for fracture propagation into the upper layer. The difference in these two pressures at either end of the offset, gives the fluid pressure loss associated with the flux across the offset.

Fig. 5 shows the evolution of P_{f1} and P_{f2} for various values of d. The solution "$d = 0$" corresponds to fracture penetration through the bedding contact and the solution "$d = \infty$" is for fracture propagation along a bedding interface without escaping. Because of viscous dissipation, a fluid lag forms and the fluid front reaches the intersection point with a delay compared with arrival of the crack tip. Results shown in Fig. 5(a) demonstrate that the existence of the fracture offset increases the fluid pressure significantly above the non-offset result. Part of the increase arises from the need to open the fracture against the higher remote vertical stress. Prior to new fracture growth, P_{f1} follows the $d = \infty$ curve. The location where each curve deviates from this flaw-free interface solution gives approximately the time of arrival of the fluid front at the secondary flaw. In Fig. 5(a), P_{f1} at large time ($\Delta t = 0.8$ s) is larger for smaller values of d. The increasing

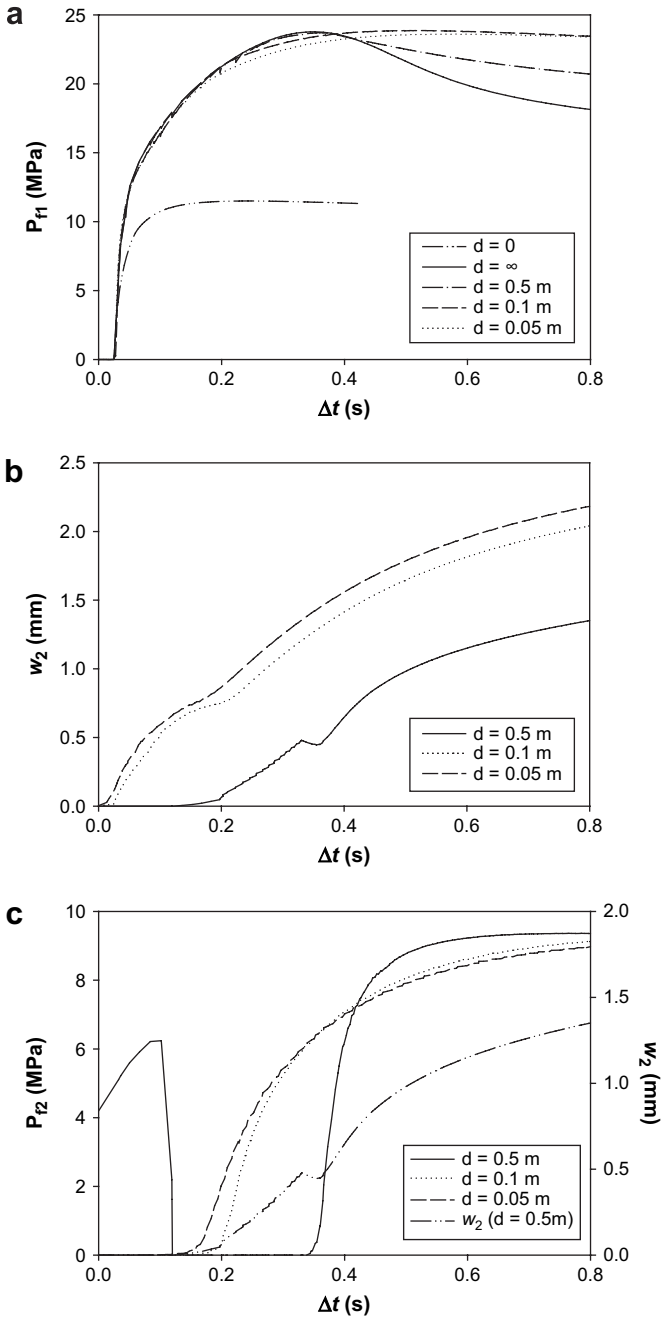

Fig. 5. Variations with time of (a) P_{f1}, (b) aperture at the flaw mouth and (c) P_{f2} for various values of d in the sandstone layers ($\mu = 0.1$ Pa s, $L = 1$ m, $\sigma^0_{xx} = 12$ MPa, $\sigma^{0(1)}_{yy} = \sigma^{0(2)}_{yy} = 5$ MPa).

trend of P_{f1} for the shorter offsets occurs because of increasing stiffness-to-opening and interaction stresses of such fracture geometries.

Flaws that are located closer to the intersection point are subjected to greater shear displacement transmitted by the parent fracture opening. This shear displacement acts to open the flaw before the fluid reaches it. Fig. 5(b) shows the rapid increase in w_2 for smaller offset sizes. The small kinking segment in each curve is associated with the arrival of the fluid front. The value of w_2 is then further increased by pressurised fluid. It is clear that for shorter offset distances, w_2 is larger.

Because the opening and the pressure are coupled, it is not easy to attribute a single cause to the wider fracture mouth. The value of w_2 is affect by the pressure in all fracture branches. Certainly, the lower parent fracture pressure and the larger offset distance both act to reduce interface slip and accordingly the opening at the entry of the daughter fracture.

The variations with time of the normal stress P_{f2} at the flaw mouth are given in Fig. 5(c) for several values of d. Fig. 5(c) also contains the curve for w_2 in the case of $d = 0.5$ m which is provided as a reference in explaining the stress and deformation states at the flaw mouth. Based on this aperture curve, the first part of the normal stress curve represents the contact stress since the new fracture is closed. The contact stresses drop to zero as the new fracture is opened by interface slip transmitted from the parent fracture aperture. The second part of the plot thus corresponds to a dry new fracture. However, interface slip cannot by itself drive the new fracture to grow far. Only after the fluid starts to fill the new fracture does the pressurised fluid drive the new fracture to propagate continuously into the upper layer. The third part of the curve shows the progressive increase of this fluid pressure. From Fig. 5(c) we conclude that the pressure P_{f2} at large time tends to be independent of values of d. Therefore, the daughter fracture growth, for the cases considered, eventually becomes independent of the stress and deformation states around the interface. The time for the arrival of the fluid front shown in Fig. 5(c) highlights the difficulty in transporting fluid through the offset at the early stage of the fracture–interface interaction. This feature is reflected in Fig. 5(c) where the curves are shifted to the right with increasing values of d.

It must be noted that the effect of fluid flow on the development of stepped natural hydraulic fractures is affected by other factors. For example, some sandstone may have higher toughness than others, although their stiffness may be only slightly different. A flaw in the layer with higher toughness may not extend. Fig. 6 shows the history of fracture aperture at Points 2 and 3 around the flaw mouth. The upper layer has a larger toughness of 2.5 MPa $\sqrt{m}$ and the offset distance is 0.5 m. In addition, the vertical *in situ* stress is reduced to 6 MPa which makes it easier for fracture growth along the bedding interface. The variation in fracture aperture at Point 2 reflects the difficulty for fluid to enter and fill the new fracture. The fracture aperture is first increased by interface slip, but it decreases after the interface at Point 3 is opened by pressurised fluid. Since the large toughness of the upper layer limits new fracture propagation, a higher fluid pressure is required to extend the flaw. However, an increase in fluid pressure can also increase the aperture and permeability along the interface. If the pressure is not sufficient to drive the new fracture to grow, the fracture will be trapped on the interface. This may explain experimental results that show soft layers with high toughness are efficient at stopping hydraulic fracture height growth (Yew, 1997). However, at $d = 0.1$ m, the flaw closer to the intersection is more easily extended with the aid of interface slip. Such a longer new fracture can significantly reduce the pressure level required for it to grow when subject to fluid pressure. In such a case, a fully-developed composite joint would be produced other than a bedding interface fracture.

Fig. 7 shows the variations with time of fracture apertures at the flaw mouth and at the starting point of the interface fracture to the left of the parent fracture (Point 4). All material parameters are the same as those used in Fig. 5, except for the vertical remote stress ($\sigma^0_{xx} = 14$ MPa). The flaw is located at 0.05 m from the intersection. The aperture at Point 4 is much smaller than that at Point 2 and more importantly, it eventually decreases to zero. The closing of the interface fracture at Point 4 has been discussed in Fig. 3(b).

4.2. Fractures in heterogeneous granite/sandstone layers

4.2.1. Contrasts of material constants

We now turn to the case of heterogeneous granite/sandstone layers where there are contrasts in Young's modulus and fracture toughness. We assume the parent fracture is hosted by the granite. We maintain the bed-parallel far-field stresses at 5 MPa in the sandstone, which requires a horizontal *in situ*

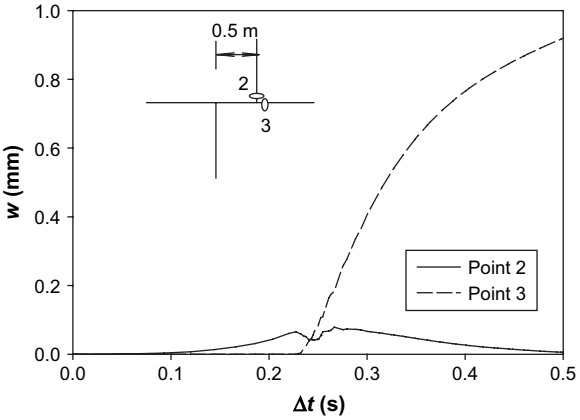

Fig. 6. Evolution of fracture apertures at Points 2 and 3 in the bedded sandstone for $d = 0.5$ m and larger fracture toughness of the upper layer $K_2^C = 2.5$ MPa$\sqrt{m}$ ($\mu = 0.1$ Pa s, $L = 1$ m, $\sigma^0_{xx} = 6$ MPa, $\sigma^{0(1)}_{yy} = \sigma^{0(2)}_{yy} = 5$ MPa).

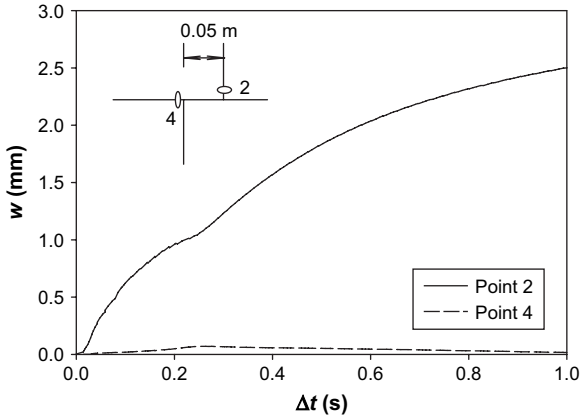

Fig. 7. Evolution of fracture aperture at Points 2 and 4 in bedded sandstone for $d = 0.05$ m and larger vertical stress $\sigma^0_{xx} = 14$ MPa ($\mu = 0.1$ Pa s, $L = 1$ m, $\sigma^{0(1)}_{yy} = \sigma^{0(2)}_{yy} = 5$ MPa).

stress of 7.88 MPa for the granite to satisfy Eq. (3). To compare these results with those for the homogeneous layer cases, the same distances of the offset are used. Fig. 8 displays the evolving normal stresses P_{f1} and P_{f2}. The general trends described in the last subsection are recovered here for heterogeneous layers. However, as shown in Fig. 8(a), the peak pressure is reached much early for this case and is higher than that for homogeneous layers, mainly owing to the fact that to create a fluid-driven joint in stiffer rocks requires a higher fluid pressure since the parent fracture is narrower. The narrower parent fracture produces less post-intersection interfacial slippage, and the fluid flow rate into the interface increases to a higher value in a shorter time. The interface fracture driven at higher pressure by a larger flux, more rapidly penetrates the offset and establishes a wider channel to the new fracture. The stiffer parent fracture is thus important in the overall fracture development and the possibility for interface pinching is minimised. Because the offset is more conductive than its counterpart for homogeneous layers at the same time, the pressure in the parent fracture decreases more quickly as shown in Fig. 8(a). The rapidly-established fracture conductivity across the offset for granite/sandstone layers is also reflected in the response of fluid pressure at the flaw mouth as shown in Fig. 8(b), as indicated by the earlier arrival of fluid front. Considering the lower values of P_{f1} and the higher value of P_{f2} at $\Delta t = 0.5$ s for heterogeneous layers, the pressure drop across the offset tends to decrease more quickly than that for the homogeneous layers.

4.2.2. Length of the parent fracture

As we saw above, fracture movement along the offset and new fracture growth depend on the opening compliance of the offset section. In particular, the stress concentration on the interface that impedes fluid flow is related to both the fracture length and the internal pressure distribution in the hydraulic fracture. Additionally, the fluid pressure and fracture aperture vary with time and location, in a manner directly related to the parent fracture length. Therefore, the effect that limits the opening over the part of the interface near the flaw must be a function of the length of the fully-developed parent joint.

Fig. 9 displays the variations of the normal stresses P_{f1} and P_{f2} with time for various values of L, when the parent fracture is located in granite. If L is larger, more fluid is required to be

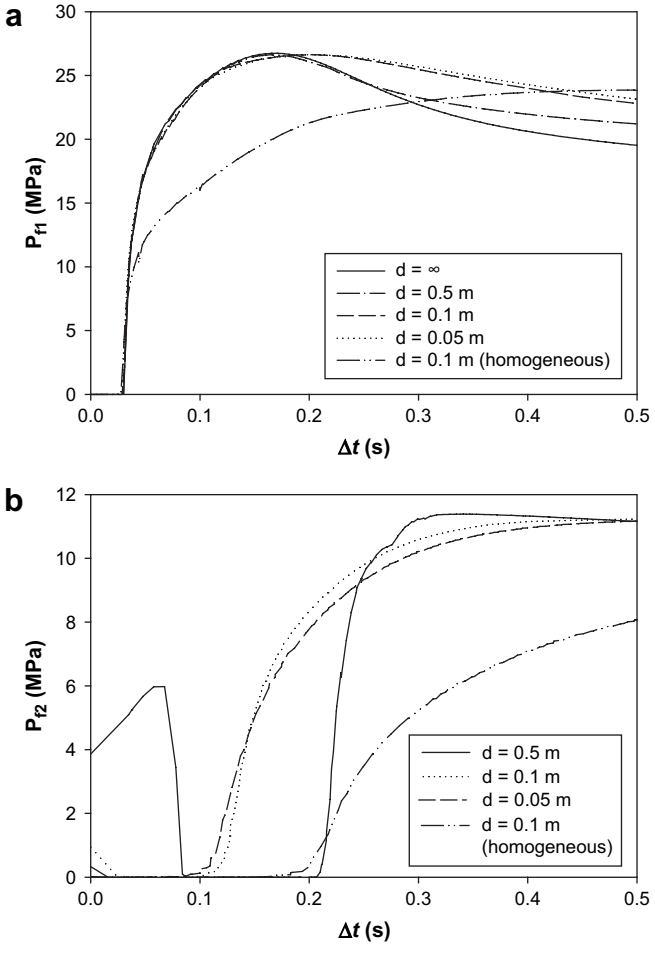

Fig. 8. Variations with time of (a) P_{f1} and (b) P_{f2} in both homogeneous and heterogeneous layers for various values of d ($\mu = 0.1$ Pa s, $L = 1$ m, $\sigma^0_{xx} = 12$ MPa, $\sigma^{0(2)}_{yy} = 5$ MPa, $\sigma^{0(1)}_{yy} = 7.88$ MPa for granite/sandstone layers and $\sigma^{0(1)}_{yy} = 5$ MPa for sandstone layers).

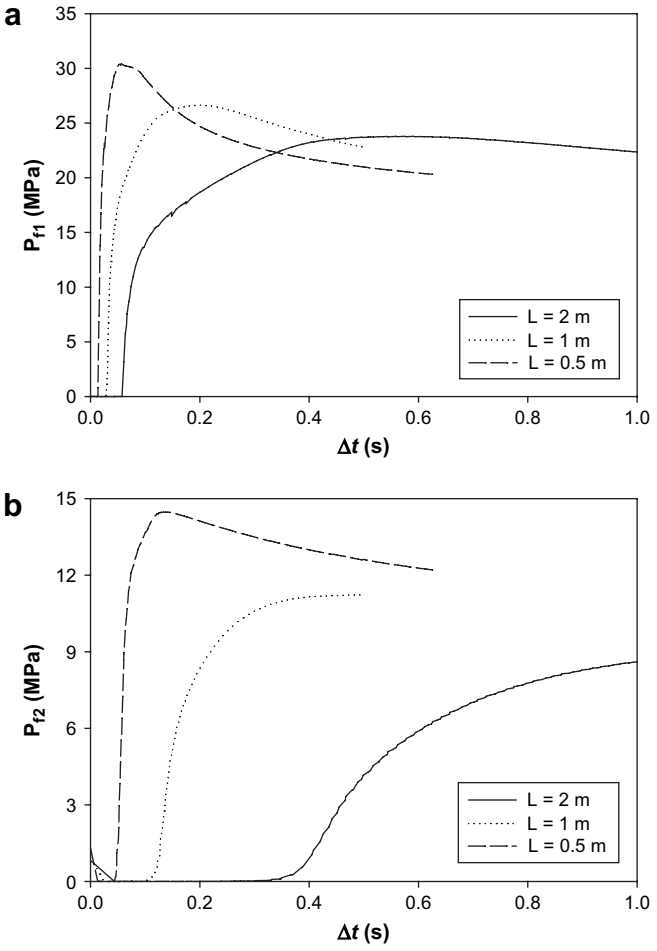

Fig. 9. Variations with time of (a) P_{f1} and (b) P_{f2} for various values of L in granite/sandstone layers ($\mu = 0.1$ Pa s, $d = 0.1$ m, $\sigma^0_{xx} = 12$ MPa, $\sigma^{0(1)}_{yy} = 7.88$ MPa and $\sigma^{0(2)}_{yy} = 5$ MPa).

injected into the system to generate the same pressure. The parent fracture growth can thus be delayed and it takes a longer time for the fluid front to reach the interface as shown in Fig. 9(a). In addition, the pressure P_{f1} increases to a lower maximum at a slower rate with increasing parent fracture length. A longer parent fracture eventually produces a wider parent fracture that generates more slip on the interface, delaying the fracture growth into the interface. This fracture–interface interaction is reflected in the slowness of fracture propagation along the offset, reflected by the later arrival of the fluid front at the flaw mouth as shown in Fig. 9(b). On the other hand, for shorter parent fractures, early-time higher pressure and flux can facilitate fracture growth along the offset and into the new fracture as discussed above. When the fluid channel is well developed, the pressure and the pressure drop over the offset decrease in time, as shown in Fig. 9. Also, the early-time higher fluid pressure at the new fracture mouth in Fig. 9(b) can drive the new fracture to grow faster. Therefore, for a shorter parent fracture, the higher pressure and influx generated can force fluids across the offset and extend the flaw more efficiently. However, a longer parent fracture is more compliant and stores more fluid volume. Flux into the interface and the new fracture is reduced by mechanical interactions and new fracture initiation is slower for this case.

For the case of $L = 2$ m, the interaction between the fractures and the interface can induce pinching on the interface near the flaw mouth as illustrated in Fig. 3(c). Fig. 10 shows the variations of fracture aperture along the interface at four times for this case. There are equal left and right interfacial fracture lengths at $\Delta t = 0.15$ s. The growth of the right branch then slows down since the interaction associated with new fracture growth causes a local stress concentration. The pinch is formed at the end of the offset because of the fracture geometry and the interaction between the branches. However, the increasing fluid pressure can propagate the left interface fracture. Prior to fluid reaching the new fracture, the left fracture length at $\Delta t = 0.37$ s is twice as long as the offset size. Meanwhile, the fluid pressure continues to increase and the pinch point starts to open. At $\Delta t = 0.5$ s, the end of the offset is opened and fluid is pressurising the daughter fracture. Our modelling shows that arrest of the fluid-filled fracture front along the offset occurs under several combinations of the parameters, as a direct result of the mechanical interaction between fractures and interface. The development of a pinch point is more likely for higher stress acting across the interface, for longer parent fractures, and for lower viscosity fluids. For the case shown in Fig. 10, P_{f1} continues to increase prior to $\Delta t = 0.5$ s as shown in Fig. 9(a). This means that an increasing pressure is needed to extend the interface fracture and open the pinching points. However, this is not always the case. In the calculations, we found that the much longer parent fracture can eventually result in closure of parts of the fracture leading to the new fracture and the left interface fracture branch then becomes wider and longer, limiting the fluid pressure increase. Hence, the pinch cannot be released and the injected fluid is stored by fracture growth on the interface.

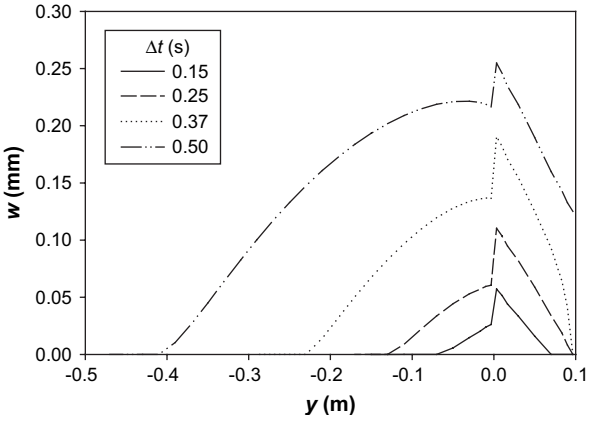

Fig. 10. Profiles of interface fracture apertures at various time instants for $L = 2$ m in granite/sandstone layers ($\mu = 0.1$ Pa s, $d = 0.1$ m, $\sigma^0_{xx} = 12$ MPa, $\sigma^{0(1)}_{yy} = 7.88$ MPa and $\sigma^{0(2)}_{yy} = 5$ MPa).

4.2.3. *In situ* stresses

It has been recognised that the stress contrasts occurring across the bedding interface play a key role in hydraulic fracture arrest or crossing (Teufel and Clark, 1984; Warpinski and Teufel, 1987; Gudmundsson and Brenner, 2001). Fig. 11

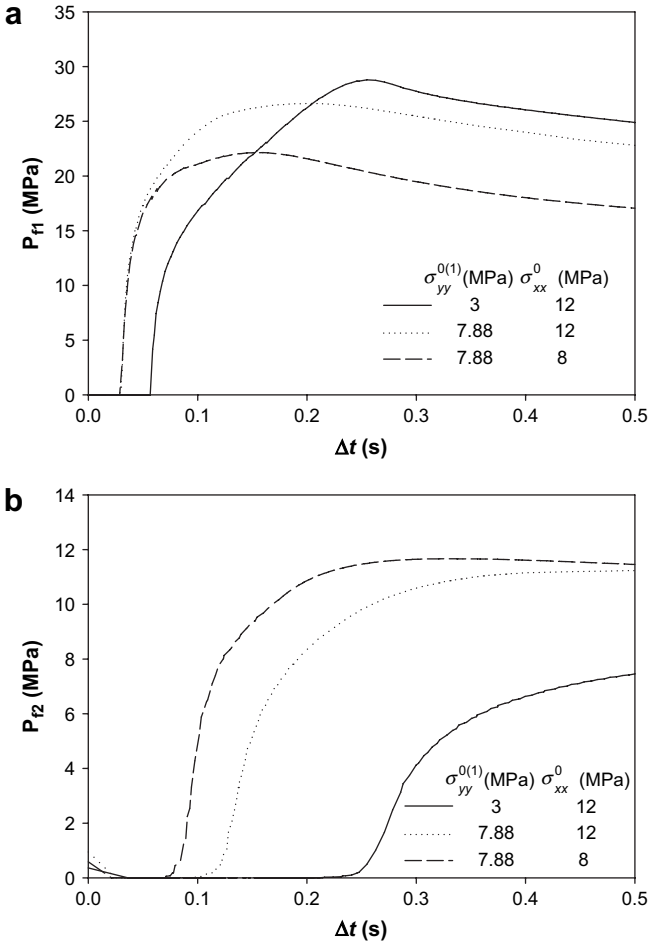

Fig. 11. Variations with time of (a) P_{f1} and (b) P_{f2} for three sets of *in situ* stresses in granite/sandstone layers ($\mu = 0.1$ Pa s, $d = 0.1$ m, $L = 1$ m).

shows the variations of P_{f1} and P_{f2} with time for three sets of the *in situ* stresses. Eq. (3) is applied, using values of $\sigma_{yy}^{0(1)}$ as shown in the figure, to determine the horizontal stress in the upper layer. From top to bottom of the legend, the stress values used for $\sigma_{yy}^{0(2)}$ are 2.56, 5.0 and 4.65 MPa. These magnitudes are also reflected in the large-time values of P_{f2} as shown in Fig. 11(b).

The fracture volume depends on the excess pressure, which is the pressure in excess of the normal stress acting across the fracture. If $\sigma_{yy}^{0(1)}$ were smaller, the parent fracture growth would occur at a correspondingly lower pressure. The lag zone is largest for $\sigma_{yy}^{0(1)} = 3$ MPa as shown in Fig. 11(a). However, for the fracture to propagate across the offset with a confining stress $\sigma_{xx}^{0} = 12$ MPa, the fluid pressure must increase to above this value. This leads to a larger excess pressure for the parent fracture if $\sigma_{yy}^{0(1)}$ is smaller. In Fig. 11(a), it takes a longer time for the injection pressure to reach the peak compared with the case of $\sigma_{yy}^{0(1)} = 7.88$ MPa. Thus, the parent fracture has a larger stored fluid volume. The mechanical interaction between the fractures and the interface leads to larger compression across the offset which impedes fracture growth. This provides an explanation for the case with $\sigma_{yy}^{0(1)} = 3$ MPa producing the highest peak pressure as shown in Fig. 11(a). A delay in fluid penetration through the offset associated with higher compression is observed in Fig. 11(b) for $\sigma_{yy}^{0(1)} = 3$ MPa. On the other hand, in the case of $\sigma_{yy}^{0(1)} = 7.88$ MPa and $\sigma_{xx}^{0} = 8$ MPa with a smaller difference of *in situ* stresses, the fracture escape becomes more efficient as reflected by a lower fluid pressure and faster fracture penetration along the offset. In short, a large difference between *in situ* stresses can slow the fracture escape process.

4.2.4. Fluid viscosity

The dynamic viscosity of fluids within the crust varies with fluid composition, temperature and pressure and can range from less than 0.001 Pa s for water, to 10^4 Pa s for basalt lava. When the injection rate is fixed, fluid pressure is sensitive to the fracture aperture. In particular, the fractures driven by extremely low-viscosity fluids have more difficulty in penetrating into the bedding interface for cases of higher vertical *in situ* stress (Zhang et al., 2007). Pinching of the offset portion of the fracture can direct the fracture growth into the interface on the left side of the parent fracture. Fig. 12 shows the variation of fracture aperture along the interface with time for $\mu = 0.01$ Pa s. Unlike the temporary pinching shown in Fig. 10, the fluid front in the offset is arrested and the fracture aperture near the flaw starts decreasing after a time of $\Delta t = 0.041$ s is reached. On the other hand, the left interface fracture branch becomes longer and its aperture becomes much greater than that along the offset. This means the fluid and fracture movement into the offset is limited and the advance of the fluid front into the new fracture becomes impossible in this case.

A larger fluid viscosity results in high fluid pressures which are needed to force the fluid through the fracture channel and especially through the narrower offset region. However, this increase in fluid pressure is associated with an increase in fracture volume and is a reflection of larger viscous energy dissipation. Results in Fig. 13 show that more time is required for the fluid-filled fracture front to reach the interface and the new fracture mouth for higher viscosity fluids. Also, the maximum values of P_{f1} and P_{f2} are larger than those for low-viscosity

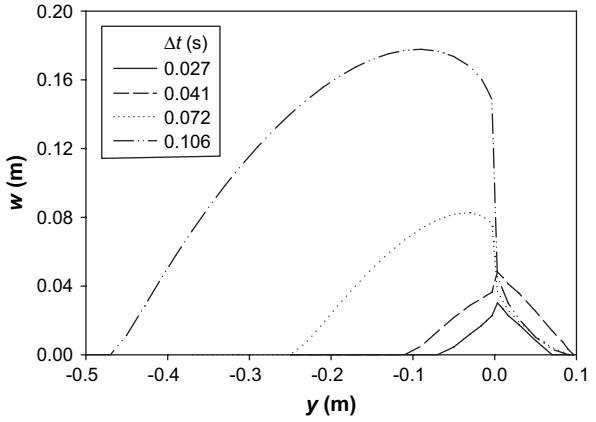

Fig. 12. Profiles of interface fracture apertures at various time instants for $\mu = 0.01$ Pa s ($d = 0.1$ m, $L = 1$ m, $\sigma_{xx}^{0} = 12$ MPa, $\sigma_{yy}^{0(1)} = 7.88$ MPa and $\sigma_{yy}^{0(2)} = 5$ MPa).

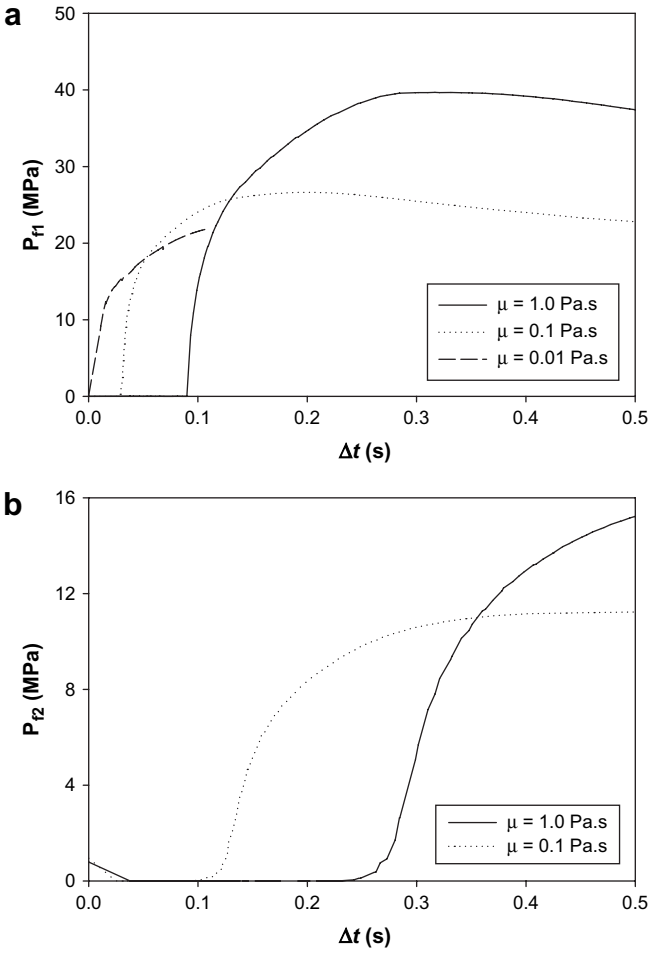

Fig. 13. Variations with time of (a) P_{f1} and (b) P_{f2} for various values of μ ($d = 0.1$ m, $L = 1$ m, $\sigma_{xx}^{0} = 12$ MPa, $\sigma_{yy}^{0(1)} = 7.88$ MPa and $\sigma_{yy}^{0(2)} = 5$ MPa).

fluids due to the larger viscous dissipation involved. These wider and highly pressurised parent and daughter fractures impose large stress concentrations across the offset, making fracture growth and fluid flow across the offset more difficult.

5. Discussion and conclusions

The numerical experiments presented in this study have explored the influence of the coupling of rock deformation and fluid flow on hydraulic fracture escape from a secondary flaw located at a random position on a bedding interface in layered rocks. The results are applied to the cases where stable crack growth is driven by a fluid injected at a constant rate. The fluid sources for driving the newly-created fracture portion can be magmas from a chamber, fracturing fluids injected by surface pumps or geofluids from the pre-existing part of the joint. The stable fracture growth is dependent on the toughness and our model cannot be applied to subcritical crack growth under cyclic or long-time loading (Lacazette and Engelder, 1992). The spatial and temporal variations of fracture opening, pressures and stresses during and after fracture crossing, which can be analysed by the hydraulic fracture propagation model presented here, play an essential role in determining how the branched fracture develops. The subsequent fracture propagation patterns depend on many factors such as rock and fluid properties, interfacial shear strength, *in situ* stresses and fracture geometry. The individual role of each influencing factor on fracture crossing of the frictional bedding interface cannot be evaluated without accounting for the local stress and deformation changes produced. In essence, numerical simulations based upon a coupled hydraulic fracture model, such as the one used for this study, are required.

In contrast to previous studies on unwetted joints, the fractures studied here are driven hydraulically. Upon intersecting the bedding interface, a fluid-driven fracture can grow along it in either direction or in both directions by overcoming the higher vertical stress and the extra compressive stress from the interaction between the interface and fractures. For all cases studied here, the growth along the interface is more difficult than in the upper and lower layers. The results presented in this paper show that the size and opening compliance of the offset portion of the composite fracture has a strong effect on the pressure in the parent fracture. A shorter offset distance is less compliant and results in a smaller offset aperture and hence a large pressure drop as fluid is forced across it. Hydraulic fractures that develop such offsets in their path require high fluid pressure to sustain fracture growth as suggested by Medlin and Fitch (1983). The offset portion of the fracture channel becomes a narrow channel and is subject to large sliding displacement. The higher pressure and the narrower channel over the offset can potentially isolate and trap the fluid-driven fracture after injection stops. These interesting features cannot be captured using uniform pressure fracture model.

In particular, from the results obtained, fracture propagation across an interface from stiff granite to soft sandstone is more likely than growth through a frictional interface in a homogeneous sandstone. The higher fluid pressure and influx to the interface generated in the stiffer granite helps establish the conductivity across the offset at an earlier time. Also, the stronger upper rock with higher toughness is found to efficiently resist fracture escape.

In addition to material constants, the fracture nucleation site on the bedding contact is an important parameter for the fracture escaping process. For the sake of simplicity, the site for fracture initiation is assumed to be known *a prior* and is taken as a secondary flaw with a small initial length in our model. This approach follows that used by other investigators (Bahat and Engelder, 1984; Helgeson and Aydin, 1991; McConaughy and Engelder, 2001; Rijken and Cooke, 2001). In this study, the interface surfaces are assumed to be strong enough to prevent any other fracture initiation on the interface. This is contradictory to the fact that the flaws under high stresses are apt to grow first. Without the above assumption, most new fractures will start from a site close to the parent fracture tip. This may explain why many crosscutting joints are found in nature (Lash and Engelder, 2005). We have recently extended our model to allow for spontaneous fracture nucleation based on a tensile stress criterion and plan to use this new version to study the issue of the location for fracture nucleation. However, the model as used here is still useful in the case where the interface is very strong, but has a pre-existing flaw. Numerical results show that if the nucleation site is closer to the intersecting point, the flaw can be extended to a significant size by interface slippage alone and the new fracture is nearly perpendicular to the bedding contact. The growth of the new fracture is faster than that for a larger offset. In addition, if the offset is larger, the larger opened interface portion at the left side of the new fracture is directly responsible for the formation of inclined new fractures.

In the layered or bedded cases, the length of the parent fracture is approximately equal to the layer thickness and can be inferred from field data. A longer parent fracture can slow the rate of pressure increase because of its larger compliance and volume. A longer time is therefore required for the fluid pressure to reach a level sufficient to open the interface and to extend a fracture through the offset. As a result, new fracture growth and fracture escape occur later and more slowly. The interaction between longer parent fractures and the interface can produce a tendency for pinching to develop along the offset.

The *in situ* stresses play a key role in the amount of fracture opening that develops along the offset and in the interaction of the hydraulic fracture with the interface. It is clear that the large difference between the vertical and the horizontal *in situ* stresses in the lower layer, hosting the parent fracture, can give rise to higher interaction stresses and more difficulty for fracture propagation along the offset portion of the interface.

The competition and interaction between fracture branches of a fluid-driven composite joint result in complex fluid flow and fracture growth patterns. The history of the resulting growth pathways and associated interactions among the branches can be evaluated using the proposed model. The evolution of fracture networks is an important issue in the geological, hydrogeological and petroleum engineering communities. Although many issues need to be clarified, the results for the

two-dimensional problems provided here can assist in the understanding of the development of hydraulic fracture networks in nature.

Acknowledgements

We thank Terry Engelder and Michele Cooke for their thorough reviews and helpful suggestions. This work was supported by the CSIRO Division of Petroleum Resources.

References

Batchelor, G.K., 1967. An Introduction to Fluid Dynamics. Cambridge University Press, Cambridge, U.K.

Bahat, D., Engelder, T., 1984. Surface morphology on cross-fold joints of the Appalachian Plateau, New York and Pennsylvania. Tectonophysics 104, 299–313.

Cooke, M.L., Underwood, C.A., 2001. Fracture termination and step-over at bedding interfaces due to frictional slip and interface opening. J. Struct. Geol. 23, 223–238.

Erdogan, F., Sih, G.C., 1963. On the crack extension in plates under plate loading and transverse shear. J. Basic Eng. 85, 519–527.

Fischer, M.P., Gross, M.R., Engelder, T., Greenfield, R.J., 1995. Finite-element analysis of the stress distribution around a pressurized crack in a layered elastic medium: implications for the spacing of fluid-driven joints in bedded sedimentary rock. Tectonophysics 247, 49–64.

Gudmundsson, A., Brenner, S.L., 2001. How hydrofractures become arrested. Terra Nova 13, 456–462.

Gross, M., 1993. The origin and spacing of cross joints: examples from Montery Formation, Santa Barbara Coastline, California. J. Struct. Geol. 15, 737–751.

He, M.Y., Bartlett, A., Evans, A.G., 1991. Kinking of a crack out of an interface: role of in-plane stress. J. Am. Ceram. Soc. 74, 767–771.

Helgeson, D.E., Aydin, A., 1991. Characteristics of joint propagation across layer interfaces in sedimentary rocks. J. Struct. Geol. 13, 897–911.

Jaeger, J.C., Cook, N.G.W., 1979. Fundamentals of Rock Mechanics. Chapman and Hall, New York.

Keer, L.M., Chen, S.H., 1981. The intersection of a pressurized crack with a joint. J. Geophys. Res. 86, 1032–1038.

Lacazette, A., Engelder, T., 1992. Fluid-driven cyclic propagation of a joint in the Ithaca siltstone, Appalachian Basin, New York. In: Evans, B., Wong, T.-F. (Eds.), Fault Mechanics and Transport Properties of Rocks. Academic Press Ltd., London, pp. 297–324.

Lash, G.G., Engelder, T., 2005. An analysis of horizontal microcracking during catagenesis: example from the Catskill Delta Complex. Am. Assoc. Pet. Geol. Bull. 89, 1433–1449.

McConaughy, D.T., Engelder, T., 2001. Joint initiation in bedded clastic rocks. J. Struct. Geol. 23, 203–221.

Medlin, W.L., Fitch, J.L., 1983. Abnormal treating pressures in MHF treatments. SPE 12108, 58th SPE Annual Technical Conference and Exhibition, San Francisco, CA, October 5–8.

Pollard, D.D., 1973. Derivation and evaluation of a mechanical model for sheet intrusions. Tectonophysics 19, 233–269.

Pollard, D.D., Aydin, A., 1988. Progress in understanding joints over the last century. Geol. Soc. Am. Bull. 100, 1181–1204.

Renshaw, C.E., Pollard, D.D., 1995. An experimentally verified criterion for propagation across unbounded frictional interfaces in brittle, linear elastic materials. Int. J. Rock Mech. Min. Sci. Geomech., 237–249.

Rice, J.R., Sih, G.C., 1965. Plane problems of cracks in dissimilar materials. J. Appl. Mech. 32, 418–423.

Rijken, P., Cooke, M.L., 2001. Role of shale thickness on vertical connectivity of fractures in the Austin Chalk, Texas: application of crack-bridging theory. Tectonophysics 337, 117–133.

Teufel, L.W., Clark, J.A., 1984. Hydraulic fracture propagation in layered rocks: experimental studies of fracture containment. Soc. Pet. Eng. J. February, 19–32.

Underwood, C.A., Cooke, M.L., Simo, J.A., Muldon, M.A., 2003. Stratigraphic controls on vertical fracture patterns in Silurian dolomite, northeastern Wisconsin. AAPG Bull. 87, 121–142.

Van As, A., Jeffrey, R.G., 2000. Caving induced by hydraulic fracturing at Northparkes Mines. In: Girard, J., et al. (Eds.), Pacific Rocks 2000: Proceedings of the Fourth North American Rock Mechanics Symposium. July 31–August 3, 2000, Seattle, Washington. A.A. Balkema, Rotterdam, the Netherlands, pp. 353–360.

Warpinski, N.R., Teufel, L.W., 1987. Influence of geologic discontinuities on hydraulic fracture propagation. J. Pet. Tech., 209–220.

Weertman, J., 1980. The stopping of a rising, liquid-filled crack in the earth's crust by a freely slipping horizontal joint. J. Geophys. Res. 85, 967–976.

Yew, C.H., 1997. Mechanics of Hydraulic Fracturing. Gulf Publishing, Houston, TX.

Zhang, X., Jeffrey, R.G., 2006. Numerical studies on crack problems in three-layered elastic media using an image method. Int. J. Fract. 139, 477–493.

Zhang, X., Jeffrey, R.G., Detournay, E., 2005. Propagation of a fluid-driven fracture parallel to the free surface of an elastic half plane. Int. J. Numer. Anal. Meth. Geomech. 29, 1317–1340.

Zhang, X., Jeffrey, R.G., Thiercelin, M., 2007. Deflection of fluid-driven fractures at bedding interfaces: a numerical investigation. J. Struct. Geol. 29, 396–410.